2011

Model Uncertainties in a Sharp Leading-Edge Hypersonic Boundary Layer

Marat Kulakhmetov
Purdue University

Alina A. Alexeenko
Purdue University - Main Campus, alexeenk@purdue.edu

49th AIAA Aerospace Sciences Meeting including the New Horizons Forum and Aerospace Exposition
4 - 7 January 2011, Orlando, Florida

AIAA 2011-1187

Model Uncertainties in a Sharp Leading-Edge Hypersonic Boundary Layer

Marat Kulakhmetov[1] and Alina Alexeenko.[2]
Purdue University, West Lafayette, IN 47906, USA

The effects of uncertainties in the gas-surface interaction and intermolecular interaction models on the hypersonic boundary layer development are investigated using the non-intrusive generalized polynomial chaos method. In particular, uncertainties in the surface shear stress, normal stress, heat flux, flowfield temperature and density resulting from uncertain viscosity exponent, surface temperature and accommodation coefficient are considered. The polynomial chaos expansion approach is used to reconstruct the probability density function, calculate mean, standard deviation and skewness of the dependent variables from the DSMC calculations. The uncertainty analysis shows that surface fluxes and flowfields in the hypersonic boundary layer are more sensitive to the accommodation coefficient than surface temperature or viscosity exponent uncertainty.

Nomenclature

a_n	=	gPC coefficient
f_z	=	PDF of the independent variable
f_y	=	PDF of the dependent variable
I	=	order of the Gaussian expansion
N	=	order of the gPC expansion
N_s	=	number of samples
T_w	=	wall temperature
w_i	=	Gaussian weight
x	=	spatial coordinate in the downstream direction
y	=	independent variable studied
$\mathbf{Y}$	=	DSMC output
z	=	independent random variable in the [-1,1] interval
$\mathbf{Z}$	=	independent random variable with an arbitrary interval
α_τ	=	momentum accommodation coefficient
γ	=	skewness of the dependent variable
λ	=	Mean Free Path (MFP)
σ	=	standard deviation of the dependent variable
ψ_n	=	orthogonal polynomial of order n
ω	=	viscosity exponent in VHS model

[1] Graduate Student, AIAA Student Member.
[2] Assistant Professor, AIAA Senior Member.

I. Introduction

Reliability and production costs of future hypersonic vehicles depend on uncertainties in critical hypersonic flow models.[1] The uncertainties in the hypersonic flow predictions stem from the variability in flight conditions, material properties, lack of high-fidelity molecular interaction models and chemical reaction models in high-enthalpy environment of hypersonic flight.[2] Gas-surface interactions in hypersonic boundary layers that describe mass, momentum and energy coupling between the gaseous and solid phases can also be a source of significant uncertainty. These interactions depend on multiple surface and flow parameters, such as surface accommodation coefficient or surface roughness. Many of these are difficult to measure and could change during flight. The uncertainty analysis of the gas-surface interaction parameters can isolate the critical parameters for future study and identify where these parameters have the greatest effect. In particular, this study presents the effects of uncertainties in the gas-surface accommodation coefficient, the surface temperature and the viscosity exponent on the hypersonic boundary layer flowfields and surface properties.

Sharp leading edge hypersonic flows are commonly divided into kinetic, transitional, strong shock-boundary layer (BL) interaction and weak shock-BL interaction regions, as is shown schematically in Fig. 1. The kinetic region is characterized by thermal and chemical non-equilibrium created by large velocities and thermal gradients. The kinetic region grows rapidly when the free stream mean free path is increased and relaxation times are decreased, which is common with increases in altitude. Direct simulation Monte Carlo (DSMC) methods[3] are required to accurately resolve the flow in the kinetic region because traditional Navier Stokes CFD codes cannot handle highly non-equilibrium flows.

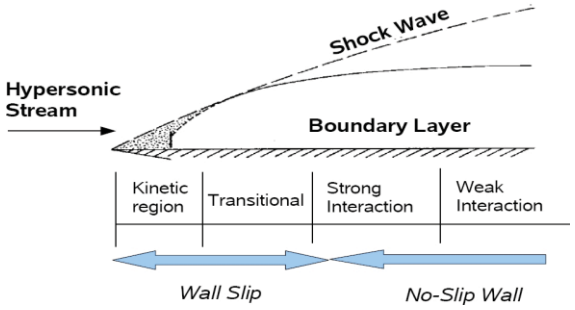

Figure 1. Schematic of a hypersonic boundary layer near a leading edge .

Both traditional uncertainty quantification (UQ) analysis and DSMC calculations are based on Monte Carlo sampling, that converge at the rate of $1/\sqrt{N_s}$, where N_s is the number of samples. Traditional UQ analysis cannot be used to study highly non-equilibrium hypersonic flows because they would require thousand of flowfield samples of the computationally expensive DSMC solutions. Instead, this study uses a non-intrusive generalized polynomial chaos expansion (gPC) that can provide accurate UQ using just three samples of the flow field computed by an unmodified DSMC code.[4,5] The gPC expansion can be represented by Eq. 1, where a_n are gPC coefficients, ψ_n are orthogonal polynomials, N is the order for the expansion, x is spatial coordinate, y is the dependent variable studied and z is the input random variable.

$$y(z,x) = \sum_{n=0}^{N-1} a_n(x)\psi_n(z) \tag{1}$$

Orthogonal polynomials in Eq.1 are selected such that their weights are equivalent to the probability distribution function (PDF) of the input parameter, $f_z(z)$. For normal input distributions [6] Hermit polynomials are used while for uniform distributions Legendre polynomials are preferred. The Legendre polynomials that are used in this study are found in table 1. Coefficients a_n, can be calculated by multiplying Eq.1 by ψ_m, computing expectations of both sides and dropping all $\psi_m\psi_n$ terms. The result of this operation is shown in Eq. 2. Since there is no known closed form relationship between z and y the expectation $\langle y\,\psi_n \rangle$ in Eq.2 has to be evaluated numerically. This can be performed using the Gauss-Legendre quadrature. The quadrature is shown on the right side of Eq.2, where I is the order of the quadrature, $\mathbf{Y}(\mathbf{Z_i}, x)$ is the DSMC output with the input random variable **Z** sampled at abscissa $\mathbf{Z_i}$, w_i is the quadrature weight that can be found in table 2 and f_z equals 1/2 . Note that the Legendre polynomials are orthogonal only on the [-1,1] interval and Gauss-Legendre quadrature is applicable only on the [-1,1] interval. If **Z**, is defined on a different interval then it needs to be rescaled to test random variable, z with a [-1, 1] interval.

TABLE (1). 3rd order Legendre Polynomials and Gauss-Legendre Quadrature

Point n or i	$\psi_n(z)$	$<\psi_n^2(z)>$	**Abscissas** z_i	**Abscissas** $\mathbf{Z_i}$	**Weights** w_i
0	1	1	$-\sqrt{\frac{3}{5}}$	$\overline{\mathbf{Z}} - \frac{(\mathbf{Z}_{\max} - \mathbf{Z}_{\min})}{2}\sqrt{\frac{3}{5}}$	5/9
1	z	1/3	0	$\overline{\mathbf{Z}}$	8/9
2	1/2 ($3z^2$-1)	1/5	$\sqrt{\frac{3}{5}}$	$\overline{\mathbf{Z}} + \frac{(\mathbf{Z}_{\max} - \mathbf{Z}_{\min})}{2}\sqrt{\frac{3}{5}}$	5/9

$$a_n(x) = \frac{<y(z,x)\psi(z)>}{<\psi_n^2(z)>} = \frac{1}{<\psi_n^2(z)>}\sum_{i=0}^{I-1}\left(\mathbf{Y}(\mathbf{Z}_i,x)\psi_n(z_i)\,f_z(z_i)w_i\right) \tag{2}$$

The mean of the studied dependent variable can be computed by taking the expectation of Eq.1. If the gPC expansion is based on Legendre polynomials then the expectation of high order terms should cancel, leaving just the first expansion coefficient, a_0, as shown in Eq.3. Standard deviation, σ, and skewness can also be computed in a similar fashion. Standard deviation and skewness of a 3rd order gPC expansion are presented in Eq. 4 and 5 respectively. In this study uncertainty is defined as a ratio of standard deviation to the mean. The PDF of the output variable, f_y, can be related to the PDF of the input variable f_z by Eq.6. The summation in Eq. 6 is over all terms z_i that lead to $y = y(z_i)$. Since 3rd order gPC expansion is quadratic, the summation in Eq.6, contains just 2 terms.

$$\bar{y}(x) = <y(z,x)> = a_0(x) \tag{3}$$

$$\sigma(x) = \sqrt{<(y(z,x)-\bar{y}(x))^2>} = \sqrt{\sum_{n=1}^{2} a_n^2(x)<\Psi_n^2(z)>} \tag{4}$$

$$\gamma(x) = \frac{<(y(z,x)-\bar{y}(x))^3>}{\sigma(x)^3} = \frac{a(x)_2^3<\psi(z)_2^3> + 3a(x)_1^2 a(x)_2 <\psi(z)_1^2\psi(z)_2^0>}{\sigma(x)^3} \tag{5}$$

$$f_y(y,x) = \sum_{i=1}^{N-1}\frac{f_z(z_i,x)}{\left|\frac{dy}{dz}(z_i,x)\right|} = \frac{f_z(z_1,x)}{\left|\frac{dy}{dz}(z_1,x)\right|} + \frac{f_z(z_2,x)}{\left|\frac{dy}{dz}(z_2,x)\right|} \tag{6}$$

The generalized polynomial chaos analysis is used to study the sensitivity of the flowfield temperature, flowfield density, surface pressure, shear and heat flux to the viscosity exponent (ω), surface momentum accommodation coefficient (α_τ), and surface temperature (T_w) of a flat plate traveling through nitrogen at Mach 10 and 20. The free stream equilibrium conditions are summarized in table 2 while the studied uncertainty parameters are presented in table 3.

TABLE (2). Free Stream Conditions

Property	**Free Stream Value**
Fluid	Nitrogen
Velocity	1400 m/s and 2814 m/s
Temperature (Trans, Vib, Rot)	47 K
Mean Free Path	0.0085 m
Pressure	6.57E-2 Pa
Density	4.6E-5 kg/m^3
Flat plate length	0.85 m (100 MFP)

The momentum accommodation coefficient is the ratio of specular to diffuse molecular reflections in the Maxwellian gas-surface interaction model. The uncertainty in the accommodation coefficient is expected to be large because the coefficient depends on surface properties, surface finish, temperature, chemistry, and molecular gas properties. Not only is this coefficient difficult to measure experimentally but it is also likely to change in flight. Experimental measurements suggest that the accommodation coefficient also varies spatially along a homogeneous flat plate. [7,8] This is discussed further in section 3C. The accommodation coefficient is varied by 33% from a mean value of 0.75 in this study . This corresponds to a 19% parameter uncertainty. Measurements made by Ramesh show that the accommodation coefficient of stainless steel and nickel in nitrogen fall in this range.[9]

Surface temperature also depends on the surface properties, the laminar-turbulent transitions, and the trajectory profiles. Uncertainty in the surface temperature is not expected to be as large as in the accommodation coefficient. The VHS viscosity exponent is often chosen such that the VHS model would accurately reproduce experimentally measured viscosities at two temperatures and approximate viscosities everywhere else. Choosing this exponent becomes difficult when the temperatures throughout the flowfield vary significantly, as is common in hypersonic flows. For example the viscosity exponent needs to be 0.74 to match viscosities of Nitrogen at 300K and 550K[10] but 0.81 to match viscosities at 300K and 120K[11]. The viscosity exponent is varied between those values in this study. This study assumes that little is known about how the accommodation coefficient, the temperature and the viscosity exponent vary in flight. Therefore, a uniform distribution is used for each dependent variable studied.

TABLE (3). Studied Surface Model Uncertainties

Property	Mean	Distribution (f_z)	Range ($\mathbf{Z}_{max} - \mathbf{Z}_{min}$)	Variation	Uncertainty
Surface Temperature	300 K	Uniform	270-330 K	10 %	6 %
Accommodation Coefficient	0.75	Uniform	0.5 - 1.0	33 %	19 %
Viscosity Exponent	0.81	Uniform	0.88-0.74	8.6%	4%

II. Numerical Approach and Verification

UQ analysis is performed on the flowfields and surface solutions obtained with the DSMC SMILE code.[12] The DSMC runs start with 260 by 60 collision and sampling cells that span 1.105 m by 0.255m in physical space. The cells are approximately half of the upstream mean free path (MFP) but are divided up to 10 times in regions of increased density. The flat plate is placed 0.255m (30 MFP) from the inflow boundary. A single species nitrogen flow is used in this study to minimize the effect of reaction rate uncertainties. Nitrogen dissociation at Mach 10 is expected to remain low because the flow temperature remains below 570K. Nitrogen dissociation can become significant at Mach 20. The VHS molecular model is used in this study. The DSMC calculations have approximately 90 computational molecules per MFP^3 and approximately 380,000 molecules in total. Each DSMC calculation takes over 6 hours to run on 8 processors and each studied independent variable requires three calculations.

Doubling the computational and physical domains in the downstream and normal directions results in a maximum of 18% variation in the flowfield temperature and 25% variation in the flowfield density. However, the peak variation due to the domain boundary is constrained in a bubble between 5 and 15 MFP above the trailing edge (TE) of the plate. The variation in the flowfield temperature and density within the first 90 MFP of the plate does not exceed 5% and 2% respectively. The variations in surface shear, normal stress and heat flux at the TE are 1.7%, 14% and 3.7% respectively. Within the first 90 MFP the surface flux variations do not exceed 0.6%. Since the domain size is kept constant in all runs during this study, variations due to the downstream boundary do not show up in the UQ analysis. The computed peak uncertainties occur further upstream or far above the plate, therefore, the errors due to the downstream boundary also do not significantly affect the UQ results.

Three microsecond time steps are used in the calculations. The calculations waited 50,000 time steps for the flowfield to reach steady state and then sampled the flowfield for 200,000 time steps. Monte Carlo sampling in SMILE results in a sampling uncertainty that scales approximately as $1/\sqrt{N_s}$, where N_s is the number of samples. Temperature and density of the flowfields sampled for 200,000 time steps differ by less than 2%, from those sampled for 800,000 time steps. Surface friction, normal stress and heat flux differ by less than 1% between the two sample sizes. Doubling the number of simulated molecules affected the flowfield and surface fluxes by less than 1% while doubling the number of collision cells resulted in the flowfield temperature variation of 2.5% but less than 0.1% variation in all other parameters. Therefore uncertainty in the flowfield temperature of less than 9%, in the flowfield density of less than 8% and in the surface fluxes of less than 2% will be considered insignificant. Note that

in this analysis a variation rather than standard deviation between a studied and a more accurate solution was reported. Numerical uncertainties (standard deviation scaled by the mean) are expected to be smaller than reported percent variations. If a higher fidelity analysis is required then numerical uncertainties could be decreased by increasing number of simulated molecules, sampling time, domain size, and collision cells.

The stagnation point heat flux PDF of Mach 10 Fay-Riddell solution, with a 10% uniform variation in the free stream temperature, produced by Monte Carlo (MC) sampling is compared to the PDF produced by a 3rd order gPC expansion. Fay-Riddell[13] is a closed form solution that could be sampled millions of time relatively quickly. Fig. 2a shows that the PDF produced by 3rd and 4th order gPC expansions match the PDF produced by MC solution with 10 million samples reasonably well but have less statistical noise. The noise in PDFs based on MC sampling increase rapidly as the sample size is decreased, as can be seen in Fig. 2b. Table 4 presents mean, standard deviation and skewness obtained from 10 million, 1 million, 100,000 MC samples, 4th, 3rd, and 2nd order gPC. Third order gPC, which requires just 3 samples, is able to reproduce the mean, standard deviation and skewness within 0.001%, 0.002% and 2.5% of a MC solution with 10 million samples. As previously discussed, the mean calculated from the three gPC expansions is equivalent to just the a_0 coefficient. The second order gPC cannot calculate skewness because skewness is a 3rd statistical moment.

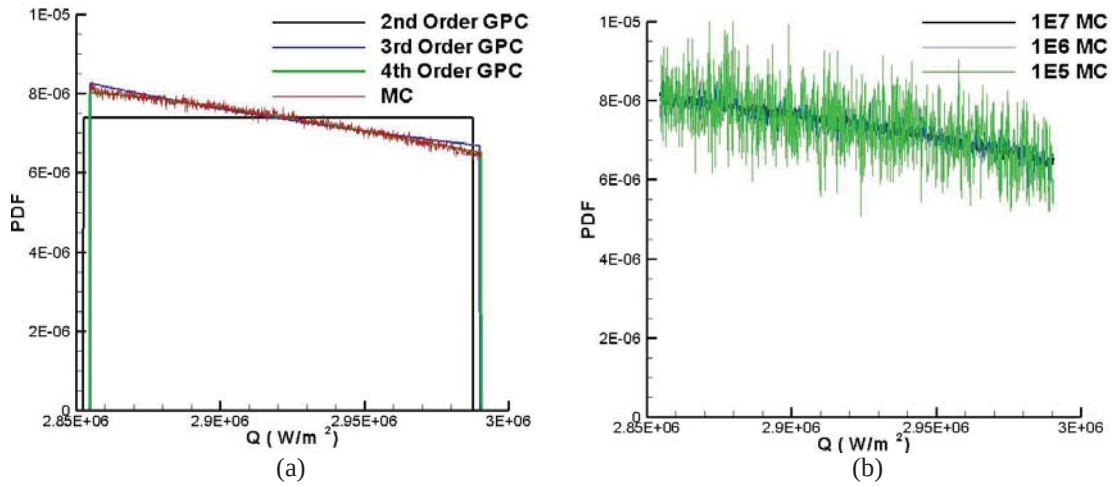

(a) (b)

Figure 2. Comparison between PDF generated by MC sampling with 10 million points and those generated by 2nd, 3rd, 4th order gPC, MC with 1 million and 10,000 sampling points..

TABLE (4). Surface Model Uncertainties

Property	Monte Carlo N = 10 million	Monte Carlo N = 1 million	Monte Carlo N = 100, 000	gPC N = 4	gPC N = 3	gPC N = 2
Mean (MW/m^2)	2.9200	2.9201	2.9200	2.9201	2.9201	2.9201
SD (MW/m^2)	0.039048	0.039049	0.039023	0.039050	0.039047	0.039033
Skewness	0.0749	0.0738	0.0697	0.0746	0.0730	0.0

III. Results and Discussion

Uncertainty in flowfield and surface fluxes due to the accommodation coefficient, surface temperature and viscosity exponent are presented below. Three DSMC calculations are used for each input parameter studied with the third order gPC. Mean, standard deviation and skewness of the output values at each spatial coordinate are calculated from Eq. 3 through 5. PDFs of the dependent variables are generated from Eq. 6. Uncertainty in this study is defined as the standard deviation divided by the mean.

A. Uncertainties in the Flowfield

A 19% uncertainty in the accommodation coefficient in the vicinity of a Mach 10 flat plate is studied first. Accommodation coefficient averaged flowfield temperature is presented in Fig. 3a., while the flowfield temperature uncertainty is presented in Fig. 3c. At this velocity the temperature reaches a maximum value of 567K approximately 21 MFP downstream of the leading edge. An 18% temperature uncertainty is generated at the LE but

propagates through the shock in two 17% uncertainty bands. Maximum temperature uncertainty of 19% is reached in the shock, 27 MFP above the TE. Along the plate temperature uncertainty drops away from LE to just 5%. The maximum, non-scaled standard deviation of 150K is found near the surface, where the temperature is highest. The averaged temperature flowfield at Mach 20 is similar to the one shown in Fig. 3a but has a peak temperature of 1948K approximately 15MFP from the leading edge. The Mach 20 temperature uncertainty flowfield is presented in Fig. 4a. At the higher velocity the temperature uncertainty propagates away from the LE through the shock and

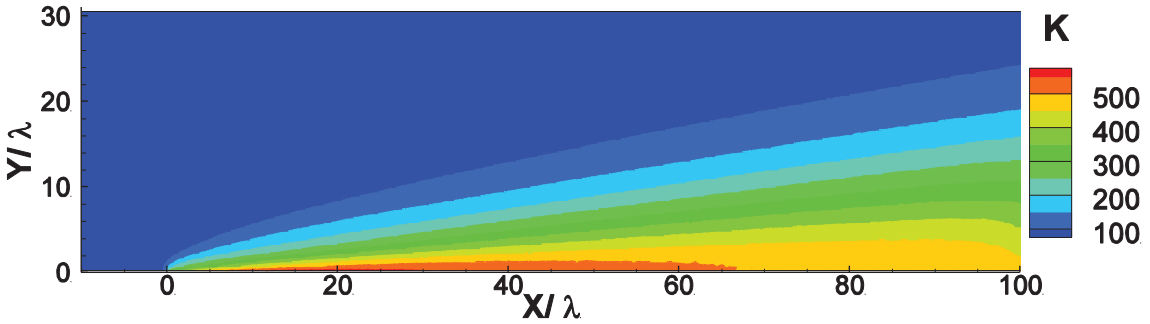

(a) Accommodation coefficient averaged Mach 10 temperature flowfield

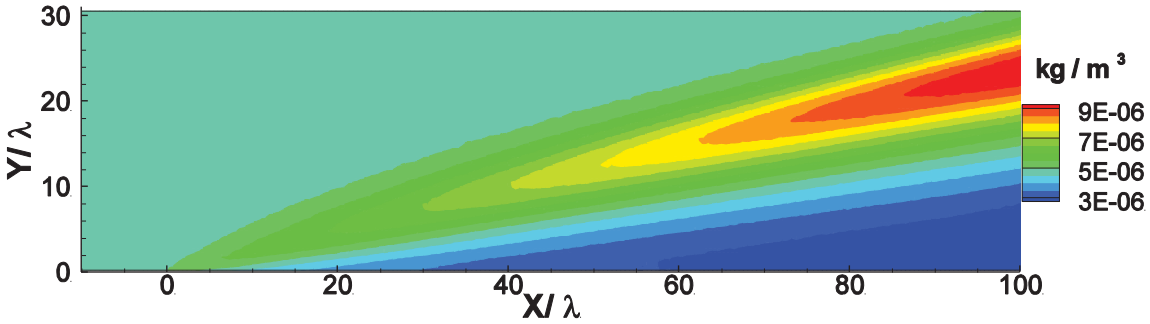

(b) Accommodation coefficient averaged Mach 10 density flowfield

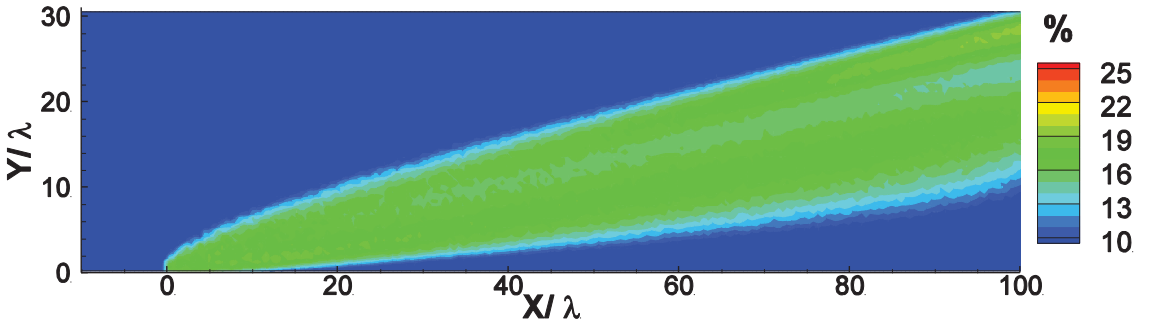

(c) Temperature uncertainty due to an uncertainty in the accommodation coefficient

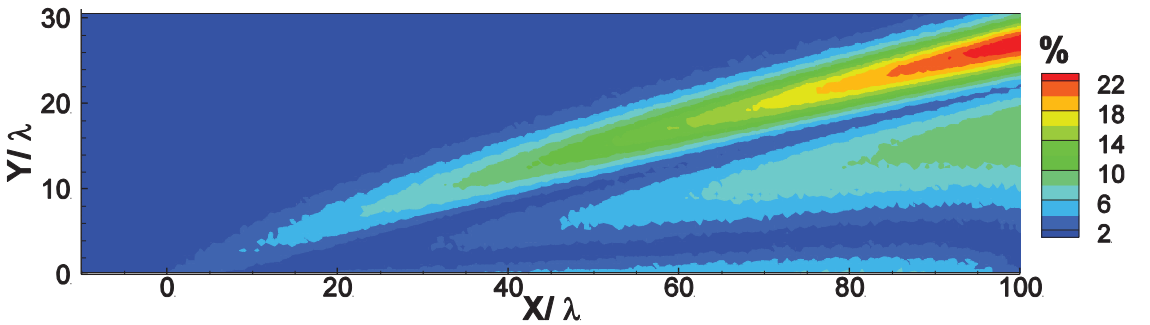

(d) Density uncertainty due to an uncertainty in the accommodation coefficient

Figure 3. Mean and uncertainty temperature and density flowfields at Mach 10

reaches a maximum of 30%, 25MFP above the TE. The maximum temperature standard deviation of 370K is found in the peak temperature region again. Uncertainties in flowfield temperature may lead to significant uncertainties in reaction rates, flowfield species concentrations and flowfield radiation.

The averaged density and density uncertainty flowfields due to the same accommodation coefficient uncertainty at Mach 10 are presented in Fig 3b and 3d respectively. Density increases along the shock and reaches a maximum value of 9.4E-6 kg/m^3 approximately 20 MFP above the plate. It decreases along the plate to a minimum value of 2.3E-6 kg/m^3. The density uncertainty increases along the shock, up to a maximum value of 24%, but remains below 5% along the plate. At Mach 20, peak density uncertainty is still found in the highest density region of the shock but its value is lowered to just 18%, as shown in Fig. 4b. Along the plate, density uncertainty increases steadily from 2% at the LE to 16%, 90MFP from the LE.

It is interesting to note that although the accommodation coefficient is uncertain only at the surface, the resultant temperature uncertainty propagates through the shock-BL interaction zone and peaks far above the surface. Increasing the accommodation coefficient decreases slip velocities and increase the shock angle. The wider shock has wide-spread effects. The accommodation coefficient uncertainty in this study result in a 30% and 38% uncertainty in the slip velocity at the two Mach numbers.
The higher shock angle then results in higher flow compression and temperature rise through the shock.

Surface temperature (T_w) and viscosity exponent (ω) averaged flowfields are similar to the accommodation coefficient averaged flowfields and therefore are not presented. At Mach 10, flowfield temperature uncertainty due T_w uncertainty is distributed nearly uniformly below the shock and remains below 3%. The density uncertainty profile due to surface temperature variation is similar to the density uncertainty profile presented in Fig. 3d but attains a maximum value of just 3%. These uncertainties are considered insignificant because they are smaller than the numerical uncertainties and input T_w uncertainty. It could be argued that the flowfields are insensitive to the surface temperature because the wall is very cold in the studied temperature range. To test this hypothesis, the surface temperature is varied again by 10% from the mean a mean wall temperature of 500K. This temperature range is close to the maximum temperature reached in the flowfield. In this case flowfield temperature and density uncertainties increased to 5% and 6% respectively but still remained insignificant. At Mach 20, the temperature

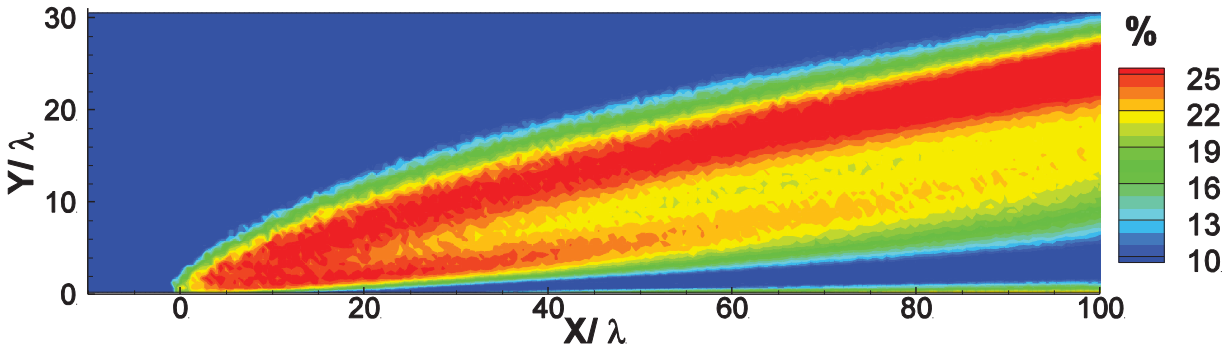

(a) Temperature uncertainty due to an uncertainty in the accommodation coefficient

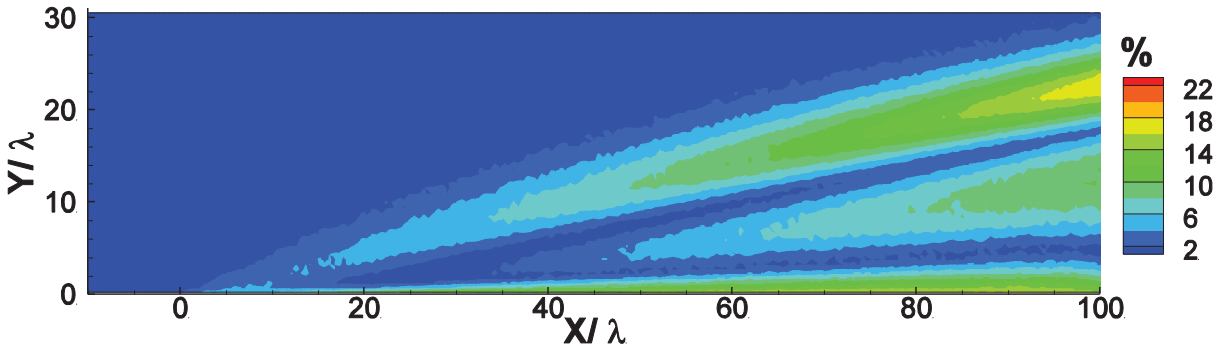

(c) Density uncertainty due to an uncertainty in the accommodation coefficient

Figure 4. Temperature and density uncertainty flowfields at Mach 20.

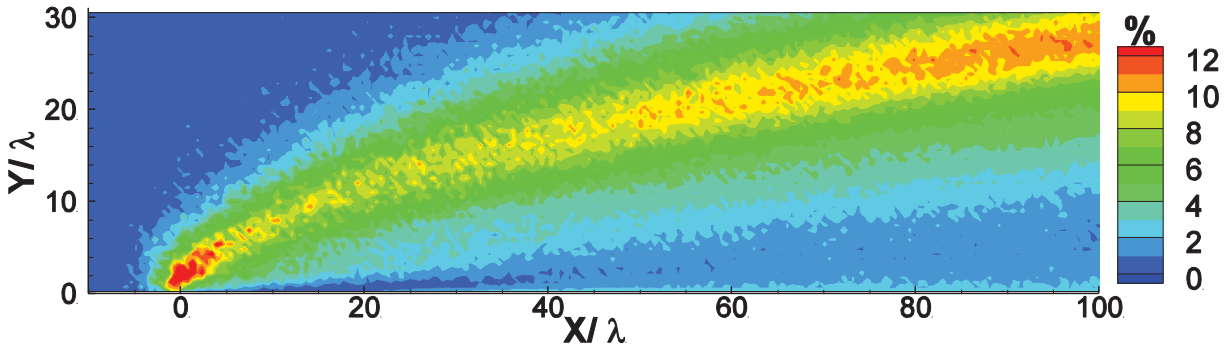

Figure 5. Temperature uncertainty due to the viscosity exponent variation.

uncertainty increases to 7% and the density uncertainty decreases to 3%. These uncertainties are still not highly significant and therefore their uncertainty profile plots are not presented in this paper.

The flowfields are also relatively insensitive to the viscosity exponent variation at Mach 10. At this velocity temperature and density uncertainties are less than 6% and 4% respectively. Raising the free stream velocity increases the temperature uncertainties to approximately 15% but maintains the density uncertainty at 4%. As shown in Fig. 5, the maximum temperature uncertainty in this trial is found at the LE but it propagated in a single band through the shock. The uncertainty due the viscosity exponent is more significant at the higher Mach number because higher Mach number flows are accompanied by higher temperature ranges. Uncertainties in the viscosity exponents also lead to a non-zero uncertainty in the free stream, as shown in fig. 5, because changing the viscosity exponent affects all molecular collision dynamics. The flowfield uncertainties are summarized in table 5.

TABLE (5). Uncertainties in the Flowfield Temperature and Density

Studied Input Parameter	Max Temp Mach 10	Max Temp Mach 10	Max Rho Mach 20	Max Rho Mach 20
Accommodation Coef. (α_τ)	19.5	30.5	24.3	17.9
Wall Temperature (T_w)	3.7	7.4	3.7	2.7
T_w, with mean at 500K	5.0		6.4	
Viscosity Exponent (ω)	5.8	15.3	3.8	4.2

B. Uncertainties in the Surface Fluxes

The accommodation coefficient averaged surface shear, normal stress and heat flux to a flat plate at Mach 10 and 20 are presented in Fig.6a, 6b and 6c respectively. Shear stress is normalized by the dynamic head, heat flux is presented as a Stanton number and normal stress is normalized by upstream pressure. The average fluxes are computed from three runs in which the accommodation coefficient is varied. Wall temperature and viscosity coefficient averaged flowfields are similar but not exact because they are sampled at slightly different abscissas. These are not presented in the paper. Shear stress and heat flux profiles attain maximum values 8 MFP from the leading edge, while normal stress attained a maximum value 28 MFP from the leading edge.

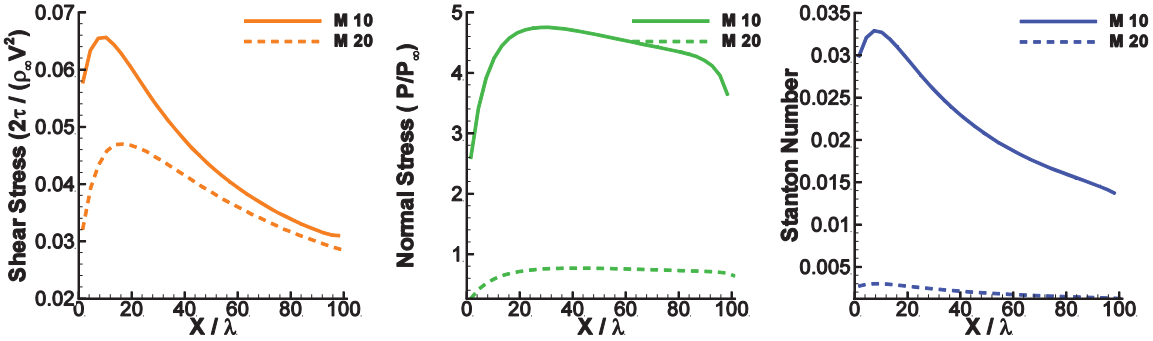

(a) Shear Stress (b) Normal Stress (c) Heat Flux

Figure 6. Shear stress, normal stress and heat flux of Mach 10 and 20 flow

Shear stress, normal stress and heat flux uncertainty profiles due to the accommodation coefficient for Mach 10 and 20 flows are presented in Fig. 4a. The three uncertainty profiles increase from the leading edge up to a maximum 4 MFP from the leading edge and then decrease again in the downstream direction. Note that traditional Navier Stokes solvers would not be able to capture peak uncertainties because they cannot resolve the flowfield within 4 MFP. As the uncertainties decrease in the downstream direction they also become negatively skewed. This is shown in Fig. 4b. At Mach 10, shear stress, normal stress and heat flux have maximum uncertainties of 22%, 16% and 22% respectively. This corresponds to 0.07 Pa, 0.04 Pa and 33 W/m^2 standard deviations. The peak shear stress and heat flux uncertainties are greater than the input accommodation coefficient uncertainty while the normal stress uncertainty is smaller. Surface uncertainties due to surface temperature and viscosity exponent remain below 3% for the entire span of the plate, as shown in Fig 4c and 4d. At Mach 20 the surface shear, normal stress and heat flux uncertainties due to the accommodation coefficient increase to 28%, 22% and 28% respectively while the uncertainties due to temperature and viscosity coefficient still remain below 1% and 5% respectively. Skewness produced by accommodation coefficient uncertainty is not significantly affected by Mach number. This statistical moment, however, appears more jagged because it is more sensitive to random DSMC noise. Skewness produced by wall temperature and viscosity exponent were not presented because uncertainties produced by these parameters were not significant. Uncertainties in the surface fluxes are summarized in table 6.

The degree of uncertainty and skewness could also be conveyed by a PDF. The Mach 20 heat flux PDF created by a uniform accommodation coefficient uncertainty is presented in Fig.8. This PDF profile first widens in the

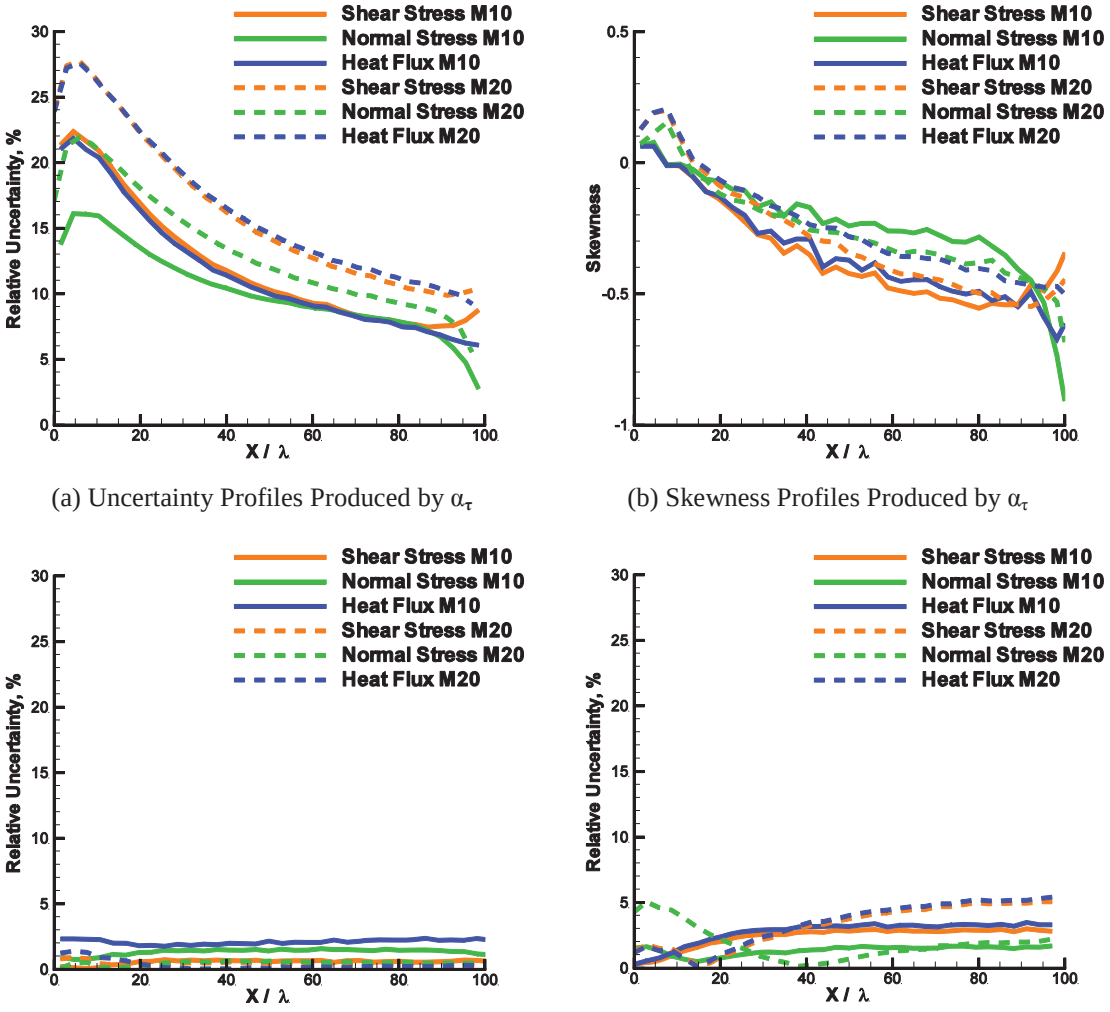

(a) Uncertainty Profiles Produced by α_τ

(b) Skewness Profiles Produced by α_τ

(c) Uncertainty Profiles Produced by T_w

(d) Skewness Profile Produced by ω

Figure 7. Uncertainty and skewness profiles for Mach 10 and 20 .

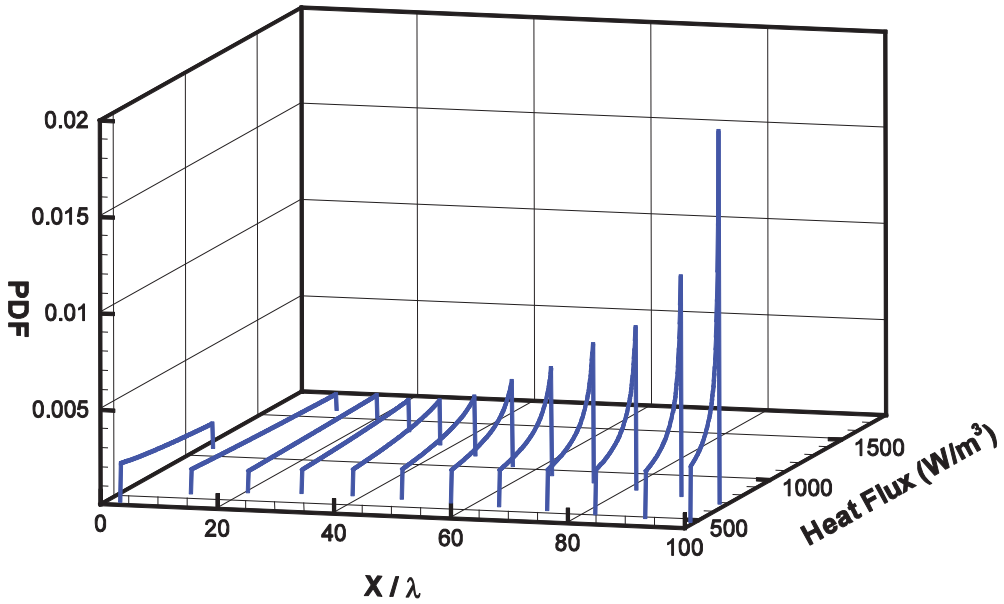

Figure 8. PDF of surface heat flux at Mach 20.

downstream direction, up to a maximum at 4 MFP from the LE, but then narrows again. The widening of the PDF signifies increased uncertainty. The profiles closer to the LE appear uniform but become negatively skewed toward the trailing edge. This negatively skewed PDF implies that the most likely heat flux value is actually higher than the mean value. Due to space constraints PDF profiles of all surface fluxes cannot be presented. The PDF profiles of other fluxes could be approximated based on uncertainty and skewness profiles presented earlier.

TABLE (6). Maximum Uncertainties in Surface Fluxes.

Surface Fluxes	Accommodation Coefficient	Surface Temperature (300K mean)	Surface Temperature (500 K Mean)	Viscosity Exponent
M10 Shear	22.4%	0.7%	0.7%	3.0%
M10 Pressure	16.1%	1.6%	1.6%	1.7%
M10 Heat Flux	21.9%	2.4%	2.4%	3.5%
M20 Shear	27.8%	0.9%	N/A	5.0%
M20 Pressure	21.9%	0.7%	N/A	5.1%
M20 Heat Flux	27.6%	1.4%	N/A	5.4%

C. Comparison with Experiments

Lengrand and co-authors, have measured normal stress and heat flux to a 0.1 m long brass plate in a Mach 20 nitrogen flow.[7] Their measurements are presented in Fig.9a and 9b. DSMC calculations for the same condition are presented in the same figure. DSMC calculations have a mean accommodation coefficient of 0.75 with a 19% uncertainty. The presented error bars span 1.0 standard deviation from the averaged flux but do not contain the experimental points near the leading edge There, it takes 3 standard deviations to capture the experimental points. This indicates that the uncertainty band in Lendrand's experiments was other than the one considered in this study. The accommodation coefficient of 1.0 provides the best match for normal stress and heat flux near the LE but after 2 cm the accommodation coefficient of 0.8 provides a better match. This shows the spatial dependence of the accommodation coefficient even for homogeneous flat plates.

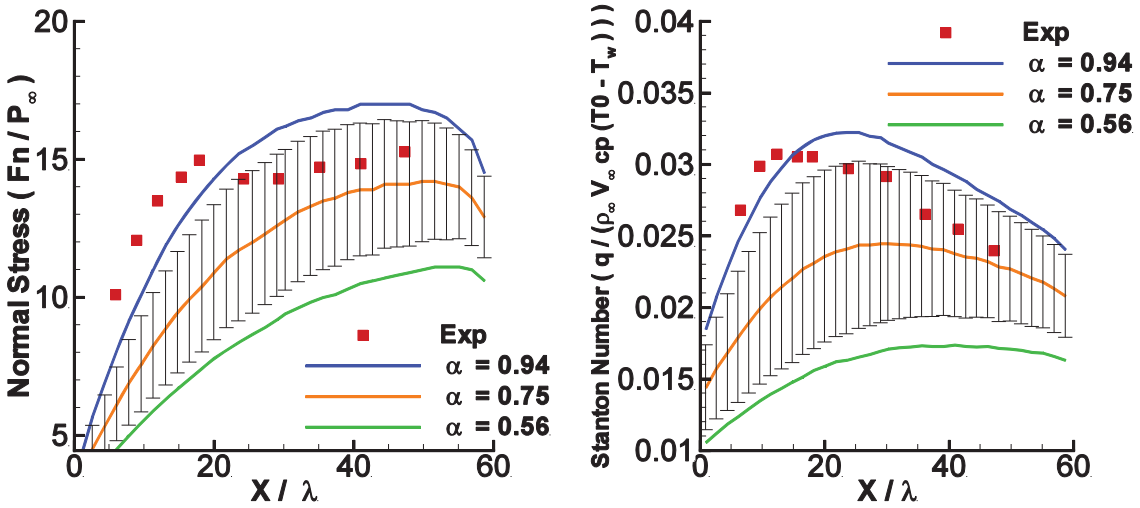

(a) Uncertainty Profiles (b) Skewness Profiles

Figure 9. DSMC comparison with experiments.

Lofthouse studied Mach 11.9 nitrogen flow above a flat plate.[8] His analysis show that near a LE an accommodation coefficient of 0.5 reproduce the experimental slip velocities accurately but an accommodation coefficient of 0.75 provides a better match 12.5 mm from the leading edge. On the other hand, the accommodation coefficient should be decreased in the downstream direction to best reproduce the normal velocity components. Unexpected surface roughness or contamination may explain why the accommodation coefficient varies in the downstream direction but this was not reported by the authors and may not be easily controlled on a hypersonic vehicle.

IV. Conclusion

A polynomial chaos expansion is used in this study to assess the sensitivity of the hypersonic boundary layer development to the momentum accommodation coefficient, the wall temperature and the viscosity exponent. Flowfield temperature, flowfield density, surface shear, heat flux and normal stress are obtained from DSMC calculations. This study shows that out of the three parameters studied, the accommodation coefficient is the most critical input parameter. At Mach 10, a 19% uncertainty in the accommodation coefficient can result in a 20% uncertainty in the flowfield temperature, 24% uncertainty in the flowfield density, 22% uncertainty in the shear stress, 16% in normal stress and 22% uncertainty in heat flux. At Mach 20 the flowfield temperature uncertainty increases to 31%, shear stress uncertainty increases to 28%, normal stress uncertainty increases to 22% , and heat flux uncertainty increases to 28% while flowfield density uncertainty drops to 18%. At Mach 20, a 4% uncertainty in the viscosity exponent can also result in a 15% uncertainty in the flowfield temperature. The flowfield and surface fluxes are not highly sensitive to uncertainties in the surface temperature.

Not only is the accommodation coefficient a highly influential parameter but its values may also change significantly along a flat plate. Lengrand has shown that the accommodation coefficient needs to decrease in the downstream to match experimental surface fluxes while Lofthouse stated that the accommodation coefficient needs to increase to match experimental slip velocities. Even though the accommodation coefficient uncertainty is introduced at the surface, the resultant uncertainties may propagate far away from the surface. Uncertainties in the flowfield temperature and density can affect the flowfield structure, reaction rates and radiation. In order to improve modeling of flows in the vicinity of sharp leading edges more effort should be devoted to accurately predicting the accommodation coefficient and improving the gas-surface interaction models

References

[1.] J.J. Bertin, R.M. Cummings, "Critical Hypersonic Aerodynamic Phenomena", Annu. Rev. Fluid Mech., 38, pp. 129-157.

[2.] Bose, D., Wright, M., and Palmer, G., "Uncertainty Analysis of Laminar Aeroheating Predictions for Mars Entries," J. Thermophysics Heat Transfer, Vol. 20, No. 4, 2006, pp. 652.

[3.] Bird, G., *Molecular gas dynamics and the direct simulation of gas flows*, Clarendon Press Oxford, 2003.

[4.] Najm, H., "Uncertainty quantification and polynomial chaos techniques in computational fluid dynamics," *Annual Review of Fluid Mechanics*, Vol. 41, 2009, pp. 35–52.

[5.] Xiu, D. and Karniadakis, G., "Modeling uncertainty in flow simulations via generalized polynomial chaos," *Journal of Computational Physics*, Vol. 187, No. 1, 2003, pp. 137–167.

[6.] Weaver, A., Alexeenko, A., R. Greendyke, J. Camberos, "Flowfield Uncertainty Analysis for Hypersonic CFD Simulations," AIAA Paper 2010-1180, 48th AIAA Aerospace Sciences Meeting, 2010..

[7.] Lengrand, JC and Allegre, J. and Chpoun, A. and Raffin, M., " Rarefied hypersonic flow over a sharp flat plate- Numerical and experimental results," Rarefied gas dynamics: Space science and engineering, 1994, pp. 276-284

[8.] Lofthouse, A.J., " Nonequilibrium hypersonic aerothermodynamics using the direct simulation Monte Carlo and Navier-Stokes models," Ph.D. Dissertation, Aeronautics and Astronautics Dept., The University of Michigan, 2008

[9.] V Ramesh and DJ Marsden, "Rotational and translational accommodation coefficients of nitrogen on nickel, silver and gold," *Vacuum*, Vol. 24, No. 7, pp. 291-294.

[10.] C. Evers, H.W. Losch, W. Wagner, " An Absolute Viscometer-Densimeter and Measurements of the Viscosity of Nitrogen, Methane, Helium, Neon, Argon, and Krypton over a Wide Range of Density and Temperature," International Journal of Thermophysics, Vol. 23, No. 6, 2002.

[11.] David W. Gough, G. Peter Mathews, E. Brian Smith, " Viscosity of Nitrogen and Certain Gaseous Mixtures at Low Temperature," Journal of the Chemical Society, Faraday Transactions 1, Vol. 72, 1976, pp.645-653

[12.] Ivanov, M., Kashkovsky, A., Gimelshein, S., Markelov, G., Alexeenko, A., Bondar YeA, Z., Nikiforov, S., and Vaschenkov, P., "SMILE System for 2D/3D DSMC Computations," Proceedings of 25th International Symposium on Rarefied Gas Dynamics, St. Petersburg, Russia, July, 2006, pp. 21–28.

[13.] Anderson, J.D.," Hypersonic and high temperature gas dynamics," AIAA, 2006